

Accepted Manuscript

Hierarchical ultrathin NiAl layered double hydroxide nanosheet arrays on carbon nanotube paper as advanced hybrid electrode for high performance hybrid capacitors

Luojiang Zhang, Rui Chen, Kwun Nam Hui, Kwan San Hui, Haiwon Lee

PII: S1385-8947(17)30854-9
DOI: <http://dx.doi.org/10.1016/j.cej.2017.05.101>
Reference: CEJ 17000

To appear in: *Chemical Engineering Journal*

Received Date: 19 February 2017
Revised Date: 16 May 2017
Accepted Date: 16 May 2017

Please cite this article as: L. Zhang, R. Chen, K.N. Hui, K.S. Hui, H. Lee, Hierarchical ultrathin NiAl layered double hydroxide nanosheet arrays on carbon nanotube paper as advanced hybrid electrode for high performance hybrid capacitors, *Chemical Engineering Journal* (2017), doi: <http://dx.doi.org/10.1016/j.cej.2017.05.101>

This is a PDF file of an unedited manuscript that has been accepted for publication. As a service to our customers we are providing this early version of the manuscript. The manuscript will undergo copyediting, typesetting, and review of the resulting proof before it is published in its final form. Please note that during the production process errors may be discovered which could affect the content, and all legal disclaimers that apply to the journal pertain.



Hierarchical ultrathin NiAl layered double hydroxide nanosheet arrays on carbon nanotube paper as advanced hybrid electrode for high performance hybrid capacitors

Luojiang Zhang ^{a,1}, Rui Chen ^{b,1}, Kwun Nam Hui ^{c,*}, Kwan San Hui ^{d,*}, Haiwon Lee ^b

^a *Department of Chemistry, Pohang University of Science and Technology (POSTECH), Pohang, Gyeongbuk 790-784, Republic of Korea*

^b *Department of Chemistry, Hanyang University, 17 Haengdang-dong, Seongdong-gu, Seoul 133-791, Republic of Korea*

^c *Institute of Applied Physics and Materials Engineering, University of Macau, Avenida da Universidade, Taipa, Macau*

^d *School of Mathematics, University of East Anglia, Norwich, NR4 7TJ, United Kingdom*

Abstract

To effectively improve the power density and rate capability of layered double hydroxide (LDH) based supercapacitors, a hybrid supercapacitor (HSC) comprising of hierarchical ultrathin NiAl-LDH nanosheet arrays on carbon nanotube paper (CNP-LDH) is developed with porous graphene nanosheets as the negative electrode for the first time. SEM image shows that hierarchical NiAl LDH nanosheet arrays are assembled by numerous ultrathin nanosheets with thickness of a few to tens of nanometers. Remarkably, with an operating voltage of 1.6 V, the

* Corresponding author.

E-mail address: bizhui@umac.mo (Kwun Nam Hui), k.hui@uea.ac.uk (Kwan San Hui)

¹ These authors contributed equally to this work.

HSC possesses a high energy density of 50.0 Wh kg^{-1} at an average power density of 467 W kg^{-1} . Even at a fast discharging time of 3.9 s , a high energy density (23.3 Wh kg^{-1}) could also be retained at a power density of 21.5 kW kg^{-1} . Moreover, the HSC exhibits cycling stability with a retention rate of 78% after 5000-cycle charge-discharge test at 5 A g^{-1} . The results inspire us to propose our high-performance CNP-LDH as a promising electrode for energy storage applications.

Keywords: Layered double hydroxide; Hybrid supercapacitor; Carbon nanotube paper; Porous graphene; Power density

1. Introduction

Supercapacitors (SCs), also called as electrochemical capacitors, have been well known for one promising energy storage device due to the high power density, fast charge/discharge capability, long lifespan, and low maintenance cost [1-4]. With these encouraging features, SCs has been adopted widely in many fields where high power density and long cycling stability are highly desirable [5, 6]. However, compared with rechargeable batteries, the energy density of commercial SCs is still too low (usually $< 10 \text{ Wh kg}^{-1}$) to come into practical applications [7]. Therefore, the development of advanced SCs with high energy density while retaining their high power density and long cycle-life is urgently sought [8, 9]. Recently, a hybrid supercapacitor (HSC), which is commonly composed of a battery-type electrode and a capacitive electrode, has been extensively investigated [10, 11]. In this case, a wider operating voltage can be achieved, which leads to a higher energy density [12, 13].

Among the various battery-type electrode materials, brucite-like layered double hydroxide (LDH) with the general formula of $[M^{II}_{1-x}M^{III}_x(OH)_2]^{x+}[A^{n-}]_{x/n}\cdot mH_2O$ have received intensive interest because of the high redox reaction activity, relatively low cost, and environmentally friendly features [14-16]. It has been reported that the electrical double-layer and Faradaic reactions can be simultaneously achieved in the abundant slabs or electrochemical active sites of the LDH structure. Therefore, LDH is regarded as promising electrode material in high performance energy storage applications [17, 18]. However, LDH suffers from its intrinsic low electrical conductivity and highly packed morphology, resulting in low rate performance and poor cycle life in supercapacitors [14, 15]. To overcome this drawback, an effective approach is to design a binder-free electrode incorporating LDH with a conductive substrates such as conductive textile fibers [19], titanium plate [20], stainless steel [21] as well as nickel foam (NF) [22, 23]. In such binder-free electrode approach, the traditional manufacture process of the slurry-derived electrode is neglected. In addition, binder-free electrode not only can effectively increase the active surface of the electroactive materials by eliminating the use of organic binder, but also facilitate faster ion and electron transport. We have demonstrated that NiAl-LDH nanosheet arrays directly grown on NF to improve the electrochemical performance for energy storage applications [12]. However, the obtained electrodes based on macro-porous metallic current collectors are usually inflexible [24]. As a result, creating an integrated electroactive flexible architecture with well-defined nanostructured possessing efficient charge and mass transportation is timely and important [25, 26].

On the other hand, among the carbonaceous materials, graphene nanosheet (GNS) has recently gained a substantial amount of attention owing to its good electrical conductivity, high theoretical specific surface area (SSA; $2630\text{ m}^2\text{ g}^{-1}$ per single layer), and excellent chemical

stability and mechanical flexibility [27-29]. However, GNS tends to aggregate and restack together due to the van der Waals interaction among graphene layers, resulting in severe decrease of the electrochemically active surface area and the access of electrolyte ions to the surface of graphene sheets. Consequently, capacitive performance is diminished drastically, particularly the rate capability and cycling stability.

Indeed, there are many papers reporting deposition of active materials on flexible substrates for supercapacitor [30, 31]. Specifically, Gao et al. developed a cotton-textile-enabled asymmetric supercapacitor in which flower-like CoAl-LDH nanoarrays were grown on activated cotton textiles using a conventional hydrothermal method [32]. However, in this manuscript, we developed a facile process to fabricate a flexible binder-free electrode, in which hierarchical ultrathin NiAl-LDH nanosheet arrays were directly grown on conductive carbon nanotube paper (CNP) by a liquid phase deposition (LPD) method for the first time, making the CNP-LDH electrode flexible enough to be repeatedly crumpled. In addition, the highly open hierarchical character of NiAl-LDH can effectively facilitate the rapid ion/electron transports, which results in excellent electrochemical performance. The obtained CNP-LDH electrode possesses a high specific capacity of up to 1023.8 C g^{-1} at a low current density of 2 A g^{-1} and 704.2 C g^{-1} even at high current density of 50 A g^{-1} , exhibiting an excellent rate performance. Using our proposed CNP-LDH as the positive electrode, an advanced HSC device can be fabricated in which porous graphene nanosheets (p-GN) serve as negative electrode material. Powdery p-GN with efficient electron and ion transport pathways as well as high SSA is synthesized via a facial hydrothermal approach. Notably, p-GN electrode delivers a specific capacitance of 209.7 F g^{-1} at 1 A g^{-1} and retains 182.3 F g^{-1} at 10 A g^{-1} with good cycling stability. Remarkably, the assembled HSC (CNP-LDH//p-GN) exhibits a high energy density of 50 Wh kg^{-1} at a power density of 467 W kg^{-1}

¹, and maintains an energy density of 23.3 Wh kg⁻¹ at a power density of 21.5 kW kg⁻¹ within a short discharging process of about 3.9 seconds. And it also represents a cycling stability with 78% specific capacity retained over 5000 continuous charge-discharge process at a current density of 5 A g⁻¹.

2. Experimental Section

2.1 Materials preparation

Synthesis of CNP-LDH composite: CNP was cleaned with deionized water and dried. The CNP-LDH was synthesized via a LPD method. Typically, a solution was firstly formed by mixing [NiF_x]^{(x-2)-} solution [14] with 10 mL H₃BO₃ (0.5 M), 2.5 mL Al(NO₃)₃·9H₂O (0.05 M), and 2.5 mL H₂O, and then sealed in a 50-mL autoclave with a piece of cleaned CNP (1 cm × 2 cm, 1.4 mg) to keep at 120 °C for 10 h. After cooled down naturally, the CNP substrate covered with NiAl-LDH was taken out from the autoclave, rinsed with water carefully, and dried overnight. The mass loading of NiAl-LDH on CNP substrate was approximately 1.0 mg which was determined by subtracting the weight before deposition from the weight after deposition.

Preparation of porous graphene nanosheets (p-GN): GO was synthesized using a modified Hummers method [15]. P-GN was prepared via a method of hydrothermal treatment. Typically, 120 mg GO was well dispersed in water by ultra-sonication to obtain homogeneous GO dispersion with a concentration of 2 mg mL⁻¹. Then, 6 mL H₂O₂ (3 vol.%) was added and stirred for 30 min. After adding 400 μL NH₃·H₂O (28 vol.%) with stirring for 30 min, the mixed dispersion was transferred to a 100-mL autoclave and maintained at 180 °C for 6 h. Finally, the p-GN powder was obtained by centrifuging, washing, and drying the resulting precipitate overnight.

2.2 Material characterizations

The phase of the samples was characterized by X-ray diffraction (XRD, Bruker D8 Advance X-ray) using Cu K α radiation ($\lambda = 0.15406$ nm) at 40 kV and 30 mA. The morphology and structures of the samples were investigated by LEO-1550 scanning electron microscopy (SEM) and JEM-2100F transmission electron microscope (TEM). A Micromeritics ASAP 2020 analyzer was used to characterize the specific surface areas (Brunauer-Emmett-Teller (BET) method) and pore structures (Barrett-Joyner-Halenda (BJH) method) of electrode materials. For CNP-LDH electrode, the LDH powder sample was scratched from the substrate by mild sonication.

2.3 Electrochemical measurement

Preparation of working electrodes: CNP-LDH composite was used as working electrode directly. For p-GN sample, the working electrode was prepared by coating the powder on NF. Typically, p-GN powder, acetylene black and polytetrafluorene-ethylene (PTFE) binder were mixed together with a weight ratio of 80: 10: 10 to obtain a homogeneous paste. The adding of acetylene black was to make up the loss conductivity caused by the introduction of binder (PTFE). After coating the aforementioned paste on a clean NF, the electrode was dried at 60 °C for 12 h before pressing under pressure of 20 MPa.

Electrochemical measurement: each electrode was first carried out in a three-electrode system using a ZIVE SP2 electrochemical working station for cyclic voltammetry (CV) and galvanostatic charge-discharge (GCD) measurements with 6 M KOH as the electrolyte. A platinum foil (1 cm \times 1 cm) and an Hg/HgO electrode were used as the counter and reference electrodes, respectively.

An HSC was assembled using the obtained CNP-LDH composite and p-GN on NF as the positive electrode and negative electrode in a 6 M KOH electrolyte solution, respectively. CV and GCD measurements were conducted in the potential range of 0 ~ 1.6 V at different scan rates and current densities, respectively.

3. Results and Discussion

3.1 Positive electrode materials (CNP-LDH)

CNP-LDH electrode material was fabricated by a facile LPD method [12]. In the presence of water and H_3BO_3 , $[\text{Ni}(\text{OH})_x]^{(x-2)-}$ was gradually grown due to the hydrolysis of the fresh Ni parent solution ($[\text{NiF}_x]^{(x-2)-}$) and will react with Al^{3+} to form NiAl-LDH nanosheets. The generation process of CNP-LDH and corresponding architectures were illuminated in Fig. 1a. The light-weight CNP substrate is beneficial for the growth of NiAl-LDH nanosheets and could serve directly as a flexible electrode for supercapacitors because of the high electrical conductivity of CNP. NiAl-LDH powders scraped from CNP-LDH composite was characterized by XRD analysis, as illustrated in Fig. 1b. It can be observed that all of the diffraction peaks are well correspond to those in the standard card (JCPDS card no: 15-0087), indicating a typical hydroxalcite-like structure [12].

The structures and morphologies of CNP and CNP-LDH were investigated by SEM. The SEM of image Fig. 2a showed that CNP is made up of a great amount of carbon nanotubes. Because of this, the CNP is high electrically conductive which is good for the growth of NiAl-LDH nanosheets active material for SC. From Fig. 2b, it can be observed that uniform NiAl-LDH nanosheets were grown on CNP substrate in the whole scene, which differed from the 3D flower-like morphology when macrosized nickel foam was used as the substrate [12]. The formation mechanism was proposed as follows: at the early stage of the reaction, the LDH

nanoplatelet nucleated and grew on individual CNT surface [33, 34]; CNTs were covered by vertically aligned LDH nanoflake arrays along with the reaction; as the reaction time was prolonged, the lateral growth of LDH were blocked by adjacent CNTs and the longitudinal growth was favorable; as a result, uniform NiAl-LDH nanosheet arrays were grown on CNP substrate. Specially, as is clear from the magnified SEM images (Fig. 2c, 2d and 2e), the as-deposited corrugated NiAl-LDH nanosheets are intertwined with each other to form a hierarchical 3-dimensional network. It is believed that such a distinct arrangement of the NiAl-LDH nanosheets can provide a high accessibility for electrolyte ions to the interior voids [35], which is benefit for the electrochemical properties. And the thin NiAl-LDH layers with a thickness of sheets ranging from a few to tens of nanometers (Fig. 2e) make more active sites expose to electrolyte ions, leading to a higher specific capacity. More detailed morphology evolution was also investigated by TEM, which showed the flake-like texture of interconnected NiAl-LDH nanosheets (Fig. 2f).

The interconnected NiAl-LDH nanosheets deposited on CNP surface formed a nanoporous structure, which was confirmed by the BET measurements in Fig. 3. As illustrated in Fig. 3a, the nitrogen adsorption-desorption isotherm of NiAl-LDH reveals a H2 type hysteresis loop, indicating the existence of a great number of pores with different sizes. From the pore size distribution plot in Fig. 3b, it can be observed that the maximum pore diameters center at the range of the mesopores (2.6 nm, 4.1 nm and 47.4 nm), which is consistent with the results of the adsorption-desorption isotherm. In addition, the sample exhibits macropores with pore sizes up to 145 nm which provide facile transport channels for electrolyte ions (OH^-) [36]. The SSA and pore volume calculated by the BJH method are $40.6 \text{ m}^2 \text{ g}^{-1}$ and $0.19 \text{ cm}^3 \text{ g}^{-1}$, respectively. The

active material with such a porous structure is favorable for the transport of electrolyte ions to their interior surface and therefore improving the electrochemical performance [14].

CV and GCD measurements were characterized to study the electrochemical properties of the prepared CNP-LDH electrode. As presented in Fig. 4a, the CV measurement was performed at scan rates of 5-100 mV s⁻¹ in the potential range of 0 to 0.6 V (vs. Hg/HgO). Two well-defined waves can be clearly observed at ~0.5 V and ~0.3 V (vs. Hg/HgO) for each curve, indicating the typical behavior of battery-type electrodes [12], which are distinct from those of a true pseudocapacitive material exhibiting rectangular-like shapes. The peaks are ascribed to the redox reaction of Ni(II)/Ni(III) based on Equation 1:[12]



When the scan rate increases, there are no significant changes in the shape of CV curves despite the movement of the redox peak positions to positive and negative direction, indicating the quasi-reversible feature of the redox couples. This means that the interfacial redox reactions are rapid enough under the given scan rates [19]. In addition, as plotted in the inset of Fig. 4a, the peak current of CNP-LDH depends on the square root of scan rates ($v^{1/2}$) linearly, confirming that the Faradaic redox reaction (Equation 1) is a quasi-reversible and diffusion control of the electrode process [12, 14]. Another attractive feature of the CNP-LDH electrode is its excellent mechanical flexibility. As shown in Fig. 4b, after crumpling into a ball, the CNP-LDH electrode can keep the original appearance and shows similar CV curve to the original profile. Fig. 4c exhibited the GCD measurement of CNP-LDH electrode at various current densities. The charge-discharge characteristics of all curves also display battery-like behavior and excellent electrochemical reversibility, consistent with the results of CV curves. The inset of Fig. 4c presented the Coulombic efficiency of the electrode as a function of current densities. The

Coulombic efficiency η , a measure of competence of charge transfer in an electrochemical reaction, were found to be 99.6%, 90.9%, 94.9%, 96.7%, 97.6%, 98.2% and 98.5%, respectively. These results suggest higher feasibility of the redox process even at higher current density conditions. The specific capacity (C) can be obtained from the discharge curves using the following Equation (2):

$$C = \frac{I \times \Delta t}{m} \dots (2)$$

where C is specific capacity ($C \text{ g}^{-1}$), I is the discharge current (A), Δt is the discharge time (s) and m is the mass of active material (LDH) in the electrode (g), respectively. The relationship of calculated C value to the current density was depicted in Fig. 4d. At a low current density of 2 A g^{-1} , the C value of CNP-LDH can reach up to 1023.8 C g^{-1} . When the current load increases to 50 A g^{-1} , the C value remains as high as 704.2 C g^{-1} (68.8% of that measured at 2 A g^{-1}). Indeed, the loading of NiAl-LDH should affect the electrical conductivity of carbon nanotube paper. In our previous paper [14], we investigated the effect of NiAl-LDH powder on another current collector such as nickel foam. The intrinsically poor conducting nature of LDH materials is the main cause of their poor performance at high current densities. Furthermore, the calculated capacity values and rate retention in this work are better than those previously reported binder-free electrodes, such as carbon textile-NiCo₂S₄ [24], LDH nanoplates/carbonate hydroxide on graphite paper [37] and ZnCo₂O₄/rGO/NiO on NF [38]. This high specific capacity and good rate performance can be ascribed to the efficient transport pathway for electrolyte ions, large active surface of NiAl-LDH and high electrical conductivity of electrode [24]. To further examine the long time stability of the electrode, a charge-discharge cycling test was first executed at 20 A g^{-1} for 5000 cycles (Fig. 4e). The specific capacity decreases from 724.8 C g^{-1} to 624.4 C g^{-1} (with a capacity retention rate of 86%) after 5000 continuous cycles. Even tested for another 5000 cycles at 50 A

g^{-1} , CNP-LDH electrode still holds a high capacitance of 591.2 C g^{-1} and about 80% of the capacity can be maintained. This intriguing observation on good cycling stability at high current densities is attributed to the structural stability of CNP-LDH electrode during the cycling tests. As confirmed from the SEM image (Fig. 4f), the original hierarchical 3D network pattern of CNP-LDH could be basically maintained after the cycling tests. In addition, the electrochemical impedance spectroscopy measurement of CNP-LDH electrode before and after cycling test was performed (inset of Fig. 4f). All spectra consist of a depressed semicircle in the high-frequency region and an oblique straight line in the low-frequency region. After the cycling test, the diameter of the semicircle for CNP-LDH was enlarged a little, suggesting the increase of charge transfer resistance and the lower interfacial contact between the NiAl-LDH nanosheets and CNP substrate during the continuous charging/discharging process [39]. The above electrochemical results directly reveal the advantages of our prepared CNP-LDH electrode such as high specific capacity, excellent rate performance and cycling stability which could make it as positive electrode in HSC.

3.2 Negative electrode materials (p-GN)

Among the various carbonaceous materials, graphene is of particular technological interest for negative electrode material in supercapacitor because of its merit of high intrinsic electrical conductivity, excellent chemical stability and high specific surface area [12]. Here, we prepared p-GN powders by a facile hydrothermal treatment of GO with simultaneous etching of pores (Fig. 5a) and then coated them with conductive agent and binder on NF to fabricate an electrode. As seen from Fig. 5b, the surface of GO is rough and a number of crumples could be observed. During the hydrothermal process at high temperature ($180 \text{ }^\circ\text{C}$), GO sheets are reduced to

graphene nanosheets. And meanwhile, the defective sites of GO could be partially etched due to the presence of H₂O₂ [40], which results in the formation of carbon vacancies and pores (Fig. 5c). From the XRD patterns (Fig. 5d), an intense peak, the (002) reflection, can be observed at 9.1° for GO, demonstrating the existence of surface oxygen-containing groups [14]. After hydrothermal treatment, the peak at 9.1° of GO disappears and a broad peak of p-GN material is observed at approximately 25.2°. The porous nature was demonstrated by nitrogen adsorption-desorption measurement (Fig. 5e). The isotherm of p-GN can be classified type IV, indicating the presence of mesopores. The SSA and pore volume of p-GN are 499.7 m² g⁻¹ and 0.31 cm³ g⁻¹, respectively. The majority of pores are narrowly distributed from 2 to 3 nm and the average pore size is 2.7 nm.

With such a distinct porous structure, p-GN is an ideal negative electrode material for use in HSC [12]. The supercapacitive behavior of p-GN electrode was first studied in a three-electrode electrochemical cell. As depicted in Fig. 6a, the CV profiles of p-GN electrode showed nearly rectangular shape under the scan rates of 5-100 mV s⁻¹ in the potential range of -1 to 0 V (vs. Hg/HgO), indicating an ideal capacitive behavior and fast charging/discharging kinetics [39]. From the GCD profiles of p-GN electrode under different current densities (Fig. 6b), it can be observed that all of the curves are ideal symmetric with no overt IR drops, illuminating the low resistance and high reversibility. The specific capacitance (*C'*) of p-GN electrode can be calculated from the discharge curves following the Equation (3):

$$C' = \frac{I \times \Delta t}{m \times \Delta V} \dots (3)$$

where *C'* is the specific capacitance (F g⁻¹), *I* is the discharge current (A), Δt is the discharge time (s) and *m* is the mass of p-GN powder in the electrode (g), respectively. Notably, the *C'* values of the electrode can reach to 209.7 F g⁻¹ at a current density of 1 A g⁻¹ and 182.3 F g⁻¹ at

10 A g⁻¹ with a good retention rate of 87% (Fig. 6c). Cycling stability of p-GN electrode was carried out by repeating 5000 charging-discharging tests at a current density of 10 A g⁻¹, as exhibited in Fig. 6d. The C' value still keeps at 184.2 F g⁻¹ after 5000 cycles, suggesting superb electrochemical stability. The results are comparable to those reported graphene materials for SCs [41], confirming the fitness of the p-GN as the negative material in HSC.

3.3 Hybrid supercapacitor (CNP-LDH//p-GN)

Considering the high capacity ability of CNP-LDH electrode (0 V ~ 0.6 V) and the rapid ionic transport feature of the p-GN material (-1 V ~ 0 V), an HSC was mounted using these two materials as the positive and negative electrodes (Scheme 1, denoted as CNP-LDH//p-GN), respectively. According to the electrochemical tests of the positive and negative electrodes in three-electrode systems, it is expected that the fabricated HSC can afford a device with a potential window of 1.6 V (Fig. 7a).

To fulfill this purpose, the charges stored in the positive and negative electrodes should be balanced according to the relationship: $Q_+ = Q_-$. And the charges stored by each electrode can be obtained by the Equation (4) and (5):

$$Q_+ = C \times m_+ \dots (4)$$

$$Q_- = C' \times m_- \times \Delta V \dots (5)$$

where C is the specific capacity of positive electrode (CNP-LDH), C' is the specific capacitance of negative electrode (p-GN), ΔV is the potential range of negative electrode during charge-discharge process, m_+ and m_- are the mass loading of active material in positive (LDH) and negative (p-GN) electrode, respectively. As a result, the mass ratio between p-GN and CNP-LDH of 5.04 is selected in the HSC.

Fig. 7b presented the CV curves of the CNP-LDH//p-GN HSC device at scan rates up to 100 mV s^{-1} in a potential range of between 0-1.6 V. Obviously, all the CV profiles differ from the desirable rectangular and display two distinct scope, that is, a narrow quasi-rectangular shape in the 0-0.7 V range and a broad redox peak in the 0.7-1.4 V region, which was widely recognized as one unique characteristic of HSC containing both the behavior of capacitive electrode (p-GN) and battery-like electrode (CNP-LDH). And the shapes shows little change when the scan rate increases to 100 mV s^{-1} , implying the fast charge-discharge property for power device. As observed from the GCD curves performed at various current densities in Fig. 7c, the symmetric charge-discharge curves imply good coulombic efficiency and superb electrochemical reversibility of our device.

The specific capacity at different current densities calculated from the discharge curves (using Equation 2) was plotted in Fig. 7d. A high specific capacity of 192.5 C g^{-1} is reached based on the total mass of active materials on the two electrodes at a current density of 0.5 A g^{-1} , and the specific capacity of HSC still remains at 78 C g^{-1} at a high current density of 20 A g^{-1} . In addition, the cycling durability of the HSC device was further performed by repeating the GCD test at a current density of 5 A g^{-1} for 5000 cycles, as exhibited in Fig. 7e. The device displays a gradually declining behavior during the first 2000 cycles and then the specific capacity almost remains unchanged in the subsequent 3000-cycle test (with a specific capacity retention of 78%), which is comparable to reported HSCs in the literature such as $\text{Ni(OH)}_2\text{-MnO}_2\text{//RGO}$ (76% after 3000 cycles) [42], $\text{NH}_4\text{NiPO}_4\cdot\text{H}_2\text{O@PPy-NF//AC}$ (71.6% after 5000 cycles) [43] and $\text{PPy@MoO}_3\text{//AC}$ (83% after 600 cycles) [44].

In order to evaluate the practical performance of our fabricated HSC, two key parameters (energy density and power density) must be investigated. Typically, they can be calculated from the following equations (6, 7):

$$E = \frac{1}{3.6} \cdot \frac{I \int V dt}{M} \dots (6)$$

$$P = 3600E/t \dots (7)$$

where E is the energy density (Wh kg^{-1}), I is the discharge current (A), M is the total active mass of both electrodes (g), $\int V dt$ is the galvanostatic discharge current area ($\text{V}\cdot\text{s}$), P is the power density (W kg^{-1}) and t is the discharge time (s). The Ragone plot describing the relationship between these two parameters of the CNP-LDH//p-GN HSC device was depicted in Fig. 7f. At a long current drain time of 385 s (current density: 0.5 A g^{-1}), the highest energy density can be calculated to be 50 Wh kg^{-1} at a power density of 467 W kg^{-1} . At a short discharge time of 6.2 s (current density: 14 A g^{-1}), the energy density can still remain 26.3 Wh kg^{-1} at the average power density of 15.3 kW kg^{-1} . Even at a current drain time as short as 3.9 s (current density: 20 A g^{-1}), the energy density can also reach 23.3 Wh kg^{-1} at a power density of 21.5 kW kg^{-1} , which is more superior than the power target of the Partnership of a New Generation of Vehicle (PNGV, 15 kW kg^{-1}) [45, 46], confirming the possibility of our prepared CNP-LDH//p-GN HSC as a power supply component in hybrid vehicle systems. In addition, the results represent that the as-obtained HSC possesses higher energy density than the reported devices such as AC//TiO₂ [47], NiCo₂O₄/Ni(OH)₂//RGO [48], AC//Li_{4-x}M_xTi_{5-y}N_yO₁₂ [49], CoNi₂S₄-NF//AC [50], NiCo₂O₄@MnO₂//AC [51], AC//H₂Ti_{12-x}Nb_xO₂₅ [52] and NiCo₂O₄@Co_xNi_{1-x}(OH)₂//CMK-3 [53].

Our fabricated CNP-LDH//p-GN HSC device can own its superior electrochemical performance to several respects: 1) As a current collector and substrate for directly deposition of

NiAl-LDH nanosheets, flexible CNP with high conductivity and excellent mechanical performance can make CNP-LDH electrode maintain mechanical integrity and high electrical conductivity. 2) Well-dispersed hierarchical porous NiAl-LDH nanosheets deposited on the surface of CNP can facilitate electrolyte ions transport to the interior surface during the rapid charge-discharge process, ensuring the effective utilization of NiAl-LDH. 3) The high SSA and nanopores of p-GN can greatly increase the ions accessible surface for improved energy storage and speed up the transport of the electrolyte ions for enhanced rate capability. The superb electrochemical performance of CNP-LDH//p-GN HSC device lays the foundation for its practical applications in electrochemical energy storage.

4. Conclusion

A flexible binder-free CNP-LDH electrode is prepared using a facile LPD method. Such highly open structure and hierarchical feature endows the electrode with superior electrochemical properties. With large ion-accessible surface area as well as efficient electron and ion transport pathways, the obtained p-GN electrode delivers high specific capacitance and good cycling stability. The fabricated HSC exhibits a cycling stability with 78% specific capacity retained after 5000 cycles at 5 A g^{-1} and achieves a high energy density of 50 Wh kg^{-1} at a power density of 467 W kg^{-1} , contributing to the high capacity and excellent rate performance of CNP-LDH and p-GN, as well as the synergistic effects of the two electrodes. Remarkably, the device maintains an energy density of 23.3 Wh kg^{-1} at a power density of 21.5 kW kg^{-1} within a short discharging process of about 3.9 seconds. Our prepared CNP-LDH electrode is expected to have special status for SC in high-performance energy storage applications.

Acknowledgements

This work was supported by the Science and Technology Development Fund from Macau SAR (FDCT-098/2015/A3), the Start-up Research Grant (SRG2015-00057-FST) from Research & Development Office at University of Macau, the UEA funding, and the MSIP (Ministry of Science, ICT and Future Planning), Korea, under the ITRC (Information Technology Research Center) support program (IITP-2015- R0992-15-1021) supervised by the IITP (Institute for Information &communications Technology Promotion).

ACCEPTED MANUSCRIPT

References

- [1] P. Simon, Y. Gogotsi, Materials for electrochemical capacitors, *Nat. Mater.*, 7 (2008) 845-854.
- [2] C. Yuan, L. Yang, L. Hou, J. Li, Y. Sun, X. Zhang, L. Shen, X. Lu, S. Xiong, X.W. Lou, Flexible Hybrid Paper Made of Monolayer Co_3O_4 Microsphere Arrays on rGO/CNTs and Their Application in Electrochemical Capacitors, *Adv. Funct. Mater.*, 22 (2012) 2560-2566.
- [3] L.F. Shen, Q. Che, H.S. Li, X.G. Zhang, Mesoporous NiCo_2O_4 Nanowire Arrays Grown on Carbon Textiles as Binder-Free Flexible Electrodes for Energy Storage, *Adv. Funct. Mater.*, 24 (2014) 2630-2637.
- [4] R.S. Ray, B. Sarma, A.L. Jurovitzki, M. Misra, Fabrication and characterization of titania nanotube/cobalt sulfide supercapacitor electrode in various electrolytes, *Chem. Eng. J.*, 260 (2015) 671-683.
- [5] T. Nguyen, S. Eugenio, M. Boudard, L. Rapenne, M.J. Carmezim, T.M. Silva, M.F. Montemor, Hybrid nickel manganese oxide nanosheet-3D metallic dendrite percolation network electrodes for high-rate electrochemical energy storage, *Nanoscale*, 7 (2015) 12452-12459.
- [6] K. Krishnamoorthy, G.K. Veerasubramani, S. Radhakrishnan, S.J. Kim, One pot hydrothermal growth of hierarchical nanostructured Ni_3S_2 on Ni foam for supercapacitor application, *Chem. Eng. J.*, 251 (2014) 116-122.
- [7] C. Ma, Y.J. Li, J.L. Shi, Y. Song, L. Liu, High-performance supercapacitor electrodes based on porous flexible carbon nanofiber paper treated by surface chemical etching, *Chem. Eng. J.*, 249 (2014) 216-225.
- [8] E. Lim, H. Kim, C. Jo, J. Chun, K. Ku, S. Kim, H.I. Lee, I.-S. Nam, S. Yoon, K. Kang, J. Lee, Advanced Hybrid Supercapacitor Based on a Mesoporous Niobium Pentoxide/Carbon as High-Performance Anode, *ACS Nano*, 8 (2014) 8968-8978.
- [9] Y.L. Xi, G.D. Wei, X.L. Liu, M.J. Pang, L.B. Liu, Y. Yang, Y. Ji, V.Y. Izotov, N.I. Klyui, W. Han, Enhancing the cycling stability of the polyaniline hybrids benefited from the hollow manganese dioxide/acetylene black skeleton, *Chem. Eng. J.*, 290 (2016) 361-370.
- [10] J.H. Kim, S.H. Lee, Use of carbon and AlPO_4 dual coating on $\text{H}_2\text{Ti}_2\text{O}_7$ anode for high stability hybrid supercapacitor, *J. Power Sources*, 331 (2016) 1-9.
- [11] B. Guan, Y. Li, B.Y. Yin, K.F. Liu, D.W. Wang, H.H. Zhang, C.J. Cheng, Synthesis of hierarchical NiS microflowers for high performance asymmetric supercapacitor, *Chem. Eng. J.*, 308 (2017) 1165-1173.
- [12] L. Zhang, K.N. Hui, K. San Hui, H. Lee, High-performance hybrid supercapacitor with 3D hierarchical porous flower-like layered double hydroxide grown on nickel foam as binder-free electrode, *J. Power Sources*, 318 (2016) 76-85.
- [13] T.W. Lin, C.S. Dai, T.T. Tasi, S.W. Chou, J.Y. Lin, H.H. Shen, High-performance asymmetric supercapacitor based on Co_9S_8 /3D graphene composite and graphene hydrogel, *Chem. Eng. J.*, 279 (2015) 241-249.
- [14] L.J. Zhang, J. Wang, J.J. Zhu, X.G. Zhang, K.S. Hui, K.N. Hui, 3D porous layered double hydroxides grown on graphene as advanced electrochemical pseudocapacitor materials, *J. Mater. Chem. A*, 1 (2013) 9046-9053.
- [15] L. Zhang, X. Zhang, L. Shen, B. Gao, L. Hao, X. Lu, F. Zhang, B. Ding, C. Yuan, Enhanced high-current capacitive behavior of graphene/ CoAl -layered double hydroxide composites as electrode material for supercapacitors, *J. Power Sources*, 199 (2012) 395-401.
- [16] H.J. Yin, Z.Y. Tang, Ultrathin two-dimensional layered metal hydroxides: an emerging platform for advanced catalysis, energy conversion and storage, *Chem. Soc. Rev.*, 45 (2016) 4873-4891.
- [17] L. Zhang, K.N. Hui, K.S. Hui, H. Lee, Facile synthesis of porous CoAl -layered double hydroxide/graphene composite with enhanced capacitive performance for supercapacitors, *Electrochim. Acta*, 186 (2015) 522-529.
- [18] R.K. Zhang, H.L. An, Z.H. Li, M.F. Shao, J.B. Han, M. Wei, Mesoporous graphene-layered double hydroxides free-standing films for enhanced flexible supercapacitors, *Chem. Eng. J.*, 289 (2016) 85-92.
- [19] G. Nagaraju, G.S.R. Raju, Y.H. Ko, J.S. Yu, Hierarchical Ni-Co layered double hydroxide nanosheets entrapped on conductive textile fibers: a cost-effective and flexible electrode for high-performance pseudocapacitors, *Nanoscale*, 8 (2016) 812-825.

- [20] S. Peng, L. Li, H.B. Wu, S. Madhavi, X.W. Lou, Controlled Growth of NiMoO₄ Nanosheet and Nanorod Arrays on Various Conductive Substrates as Advanced Electrodes for Asymmetric Supercapacitors, *Adv. Energy Mater.*, (2014) 1401172-1401178.
- [21] L. Qian, W. Chen, M.M. Liu, Q.N. Jia, D. Xiao, One-Step Electrodeposition of S-Doped Cobalt-Nickel Layered Double Hydroxides on Conductive Substrates and their Electrocatalytic Activity in Alkaline Media, *Chemelectrochem*, 3 (2016) 950-958.
- [22] Y. Bai, W.Q. Wang, R.R. Wang, J. Sun, L. Gao, Controllable synthesis of 3D binary nickel-cobalt hydroxide/graphene/nickel foam as a binder-free electrode for high-performance supercapacitors, *J. Mater. Chem. A*, 3 (2015) 12530-12538.
- [23] B. Wang, Q. Liu, Z.Y. Qian, X.F. Zhang, J. Wang, Z.S. Li, H.J. Yan, Z. Gao, F.B. Zhao, L.H. Liu, Two steps in situ structure fabrication of Ni-Al layered double hydroxide on Ni foam and its electrochemical performance for supercapacitors, *J. Power Sources*, 246 (2014) 747-753.
- [24] L. Hao, L.F. Shen, J. Wang, Y.L. Xu, X.G. Zhang, Hollow NiCo₂S₄ nanotube arrays grown on carbon textile as a self-supported electrode for asymmetric supercapacitors, *RSC Adv.*, 6 (2016) 9950-9957.
- [25] Y.S. Yesi, I. Shown, A. Ganguly, T.T. Ngo, L.C. Chen, K.H. Chen, Directly-Grown Hierarchical Carbon Nanotube@Polypyrrole Core-Shell Hybrid for High-Performance Flexible Supercapacitors, *Chemsuschem*, 9 (2016) 370-378.
- [26] M. Cakici, K.R. Reddy, F. Alonso-Marroquin, Advanced electrochemical energy storage supercapacitors based on the flexible carbon fiber fabric-coated with uniform coral-like MnO₂ structured electrodes, *Chem. Eng. J.*, 309 (2017) 151-158.
- [27] C.Z. Yuan, L. Zhou, L.R. Hou, Facile fabrication of self-supported three-dimensional porous reduced graphene oxide film for electrochemical capacitors, *Materials Letters*, 124 (2014) 253-255.
- [28] K. Gopalsamy, J. Balamurugan, T.D. Thanh, N.H. Kim, J.H. Lee, Fabrication of nitrogen and sulfur co-doped graphene nanoribbons with porous architecture for high-performance supercapacitors, *Chem. Eng. J.*, 312 (2017) 180-190.
- [29] H. Yin, S. Zhao, J. Wan, H. Tang, L. Chang, L. He, H. Zhao, Y. Gao, Z. Tang, Three-dimensional graphene/metal oxide nanoparticle hybrids for high-performance capacitive deionization of saline water, *Adv. Mater.*, 25 (2013) 6270-6276.
- [30] S. Zheng, X. Tang, Z.S. Wu, Y.Z. Tan, S. Wang, C. Sun, H.M. Cheng, X. Bao, Arbitrary-Shaped Graphene-Based Planar Sandwich Supercapacitors on One Substrate with Enhanced Flexibility and Integration, *ACS Nano*, 11 (2017) 2171-2179.
- [31] Z. Li, M. Shao, L. Zhou, R. Zhang, C. Zhang, J. Han, M. Wei, D.G. Evans, X. Duan, A flexible all-solid-state micro-supercapacitor based on hierarchical CuO@layered double hydroxide core-shell nanoarrays, *Nano Energy*, 20 (2016) 294-304.
- [32] Z. Gao, C. Bumgardner, N. Song, Y. Zhang, J. Li, X. Li, Cotton-textile-enabled flexible self-sustaining power packs via roll-to-roll fabrication, *Nat Commun*, 7 (2016) 11586.
- [33] H.Y. Chen, F. Cai, Y.R. Kang, S. Zeng, M.H. Chen, Q.W. Li, Facile Assembly of Ni-Co Hydroxide Nanoflakes on Carbon Nanotube Network with Highly Electrochemical Capacitive Performance, *ACS Appl. Mater. Inter.*, 6 (2014) 19630-19637.
- [34] H.Y. Chen, Y.R. Kang, F. Cai, S. Zeng, W.W. Li, M.H. Chen, Q.W. Li, Electrochemical conversion of Ni₂(OH)₂CO₃ into Ni(OH)₂ hierarchical nanostructures loaded on a carbon nanotube paper with high electrochemical energy storage performance, *J. Mater. Chem. A*, 3 (2015) 1875-1878.
- [35] X. Wang, C.Y. Yan, A. Sumboja, J. Yan, P.S. Lee, Achieving High Rate Performance in Layered Hydroxide Supercapacitor Electrodes, *Adv. Energy Mater.*, 4 (2014) 1301240-1301246.
- [36] H.S. Li, X.Y. Wang, B. Ding, G. Pang, P. Nie, L.F. Shen, X.G. Zhang, Enhanced Lithium-Storage Performance from Three-Dimensional MoS₂ Nanosheets/Carbon Nanotube Paper, *Chemelectrochem*, 1 (2014) 1118-1125.
- [37] J. Yang, C. Yu, X. Fan, J. Qiu, 3D Architecture Materials Made of NiCoAl-LDH Nanoplates Coupled with NiCo-Carbonate Hydroxide Nanowires Grown on Flexible Graphite Paper for Asymmetric Supercapacitors, *Adv. Energy Mater.*, 4 (2014) 1400761-1400768.

- [38] S. Sahoo, J.-J. Shim, Facile Synthesis of Three-Dimensional Ternary ZnCo₂O₄/Reduced Graphene Oxide/NiO Composite Film on Nickel Foam for Next Generation Supercapacitor Electrodes, *Acs Sustain Chem Eng*, 5 (2017) 241-251.
- [39] H. Tang, J. Wang, H. Yin, H. Zhao, D. Wang, Z. Tang, Growth of polypyrrole ultrathin films on MoS₂ monolayers as high-performance supercapacitor electrodes, *Adv. Mater.*, 27 (2015) 1117-1123.
- [40] Y.X. Xu, Z.Y. Lin, X. Zhong, X.Q. Huang, N.O. Weiss, Y. Huang, X.F. Duan, Holey graphene frameworks for highly efficient capacitive energy storage, *Nat. Commun.*, 5 (2014) 4554-4561.
- [41] N. Yu, H. Yin, W. Zhang, Y. Liu, Z.Y. Tang, M.Q. Zhu, High-Performance Fiber-Shaped All-Solid-State Asymmetric Supercapacitors Based on Ultrathin MnO₂ Nanosheet/Carbon Fiber Cathodes for Wearable Electronics, *Adv. Energy Mater.*, 6 (2016) 1501458-1501466.
- [42] H. Chen, L.F. Hu, Y. Yan, R.C. Che, M. Chen, L.M. Wu, One-Step Fabrication of Ultrathin Porous Nickel Hydroxide-Manganese Dioxide Hybrid Nanosheets for Supercapacitor Electrodes with Excellent Capacitive Performance, *Adv. Energy Mater.*, 3 (2013) 1636-1646.
- [43] C. Chen, N. Zhang, X.H. Liu, Y.L. He, H. Wan, B. Liang, R.Z. Ma, A.Q. Pan, V.A.L. Roy, Polypyrrole-Modified NH₄NiPO₄ center dot H₂O Nanoplate Arrays on Ni Foam for Efficient Electrode in Electrochemical Capacitors, *Acs Sustain Chem Eng*, 4 (2016) 5578-5584.
- [44] Y. Liu, B.H. Zhang, Y.Q. Yang, Z. Chang, Z.B. Wen, Y.P. Wu, Polypyrrole-coated alpha-MoO₃ nanobelts with good electrochemical performance as anode materials for aqueous supercapacitors, *J. Mater. Chem. A*, 1 (2013) 13582-13587.
- [45] D.W. Wang, F. Li, M. Liu, G.Q. Lu, H.M. Cheng, 3D aperiodic hierarchical porous graphitic carbon material for high-rate electrochemical capacitive energy storage, *Angew Chem Int Edit*, 47 (2008) 373-376.
- [46] Z.J. Fan, J. Yan, T. Wei, L.J. Zhi, G.Q. Ning, T.Y. Li, F. Wei, Asymmetric Supercapacitors Based on Graphene/MnO₂ and Activated Carbon Nanofiber Electrodes with High Power and Energy Density, *Adv. Funct. Mater.*, 21 (2011) 2366-2375.
- [47] H.-J. Choi, J.H. Kim, H.-K. Kim, S.-H. Lee, Y.-H. Lee, Improving the Electrochemical Performance of Hybrid Supercapacitor using Well-organized Urchin-like TiO₂ and Activated Carbon, *Electrochim. Acta*, 208 (2016) 202-210.
- [48] X.S. Yin, C.H. Tang, L.Y. Zhang, Z.G. Yu, H. Gong, Chemical insights into the roles of nanowire cores on the growth and supercapacitor performances of Ni-Co-O/Ni(OH)₂ core/shell electrodes, *Sci. Rep.*, 6 (2016) 21566-21577.
- [49] H.-K. Kim, S.-H. Lee, Enhanced electrochemical performances of cylindrical hybrid supercapacitors using activated carbon/ Li_{4-x}M_xTi_{5-y}NyO₁₂ (M=Na, N=V, Mn) electrodes, *Energy*, 109 (2016) 506-511.
- [50] W. Hu, R.Q. Chen, W. Xie, L.L. Zou, N. Qin, D.H. Bao, CoNi₂S₄ Nanosheet Arrays Supported on Nickel Foams with Ultrahigh Capacitance for Aqueous Asymmetric Supercapacitor Applications, *ACS Appl. Mater. Inter.*, 6 (2014) 19318-19326.
- [51] S. Khalid, C.B. Cao, L. Wang, Y.Q. Zhu, Microwave Assisted Synthesis of Porous NiCo₂O₄ Microspheres: Application as High Performance Asymmetric and Symmetric Supercapacitors with Large Areal Capacitance, *Sci. Rep.*, 6 (2016) 22699-22711.
- [52] J.H. Lee, H.-K. Kim, E. Baek, M. Pecht, S.-H. Lee, Y.-H. Lee, Improved performance of cylindrical hybrid supercapacitor using activated carbon/ niobium doped hydrogen titanate, *J. Power Sources*, 301 (2016) 348-354.
- [53] K.B. Xu, R.J. Zou, W.Y. Li, Q. Liu, X.J. Liu, L. An, J.Q. Hu, Design and synthesis of 3D interconnected mesoporous NiCo₂O₄@Co_xNi_{1-x}(OH)₂ core-shell nanosheet arrays with large areal capacitance and high rate performance for supercapacitors, *J. Mater. Chem. A*, 2 (2014) 10090-10097.

Captions of Figures

Fig. 1 (a) Schematic illustration of the synthesis of flexible CNP-LDH material. (b) XRD pattern of NiAl-LDH scraped from CNP-LDH material by mild sonication.

Fig. 2 Typical SEM images of (a) CNP and (b-e) CNP-LDH, and (f) TEM image of NiAl-LDH scraped from CNP-LDH by mild sonication.

Fig. 3 (a) The nitrogen adsorption-desorption isotherm loop and (b) the pore size distribution data of NiAl-LDH scraped from CNP-LDH by mild sonication.

Fig. 4 (a) CV curves of CNP-LDH electrode at various scan rates (inset: relationship of peak current with scan rate). (b) Comparison of CV curves of CNP-LDH electrode and after crumpling into a ball (scan rate: 5 mV s^{-1}). (c) GCD curves of CNP-LDH electrode at different current densities (inset: Coulombic efficiency of CNP-LDH electrode at different current densities). (d) Correlation between the specific capacity values and current density of CNP-LDH electrode. (e) Cycling performance of the electrode at current densities of 20 A g^{-1} and 50 A g^{-1} for 5000 cycles, respectively. (f) SEM image of CNP-LDH electrode after the cycling stability test (inset: electrochemical impedance spectra of CNP-LDH before and after cycling test).

Fig. 5 (a) Schematic illustration of the synthesis of p-GN material. Typical TEM and SEM images of (b) GO and (c) p-GN. (d) XRD pattern of GO and p-GN. (e) The nitrogen sorption isotherm loop and the pore size distribution data of p-GN.

Fig. 6 (a) CV curves of p-GN electrode at various scan rates. (b) Charge-discharge curves of p-GN electrode at different current densities. (c) Specific capacitance of p-GN electrode at different current densities. (d) Cycling stability of p-GN electrodes at 10 A g^{-1} for 5000 cycles.

Scheme 1 The HSC made of CNP-LDH (positive electrode) // p-GN (negative electrode).

Fig. 7 (a) CV curves of CNP-LDH and p-GN in a three-electrode system at a scan rate of 10 mV s^{-1} . (b) CV curves of CNP-LDH//p-GN HSC device at different scan rates. (c) GCD curves and (d) specific capacity of HSC device at different current densities. (e) Cycling performance of HSC device at 5 A g^{-1} for 5000 cycles. (f) Ragone plot of energy and power density of HSC device at various charge-discharge rates.

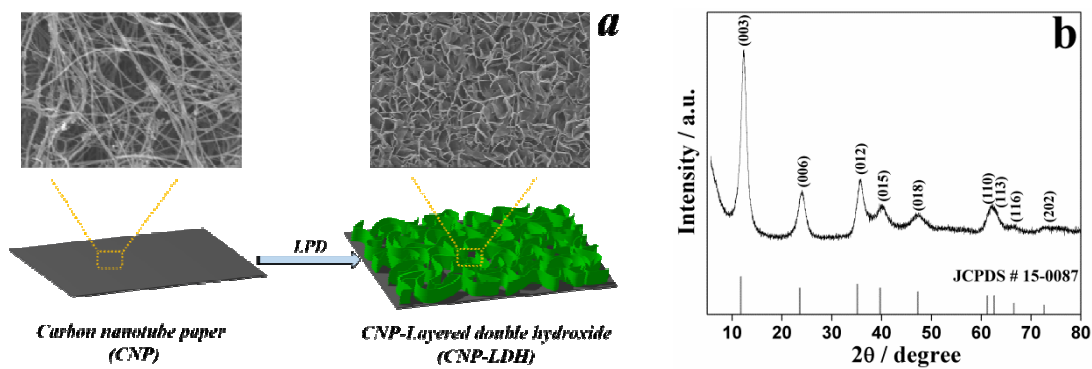


Fig. 1 (a) Schematic illustration of the synthesis of flexible CNP-LDH material. (b) XRD pattern of NiAl-LDH scraped from CNP-LDH material by mild sonication.

ACCEPTED MANUSCRIPT

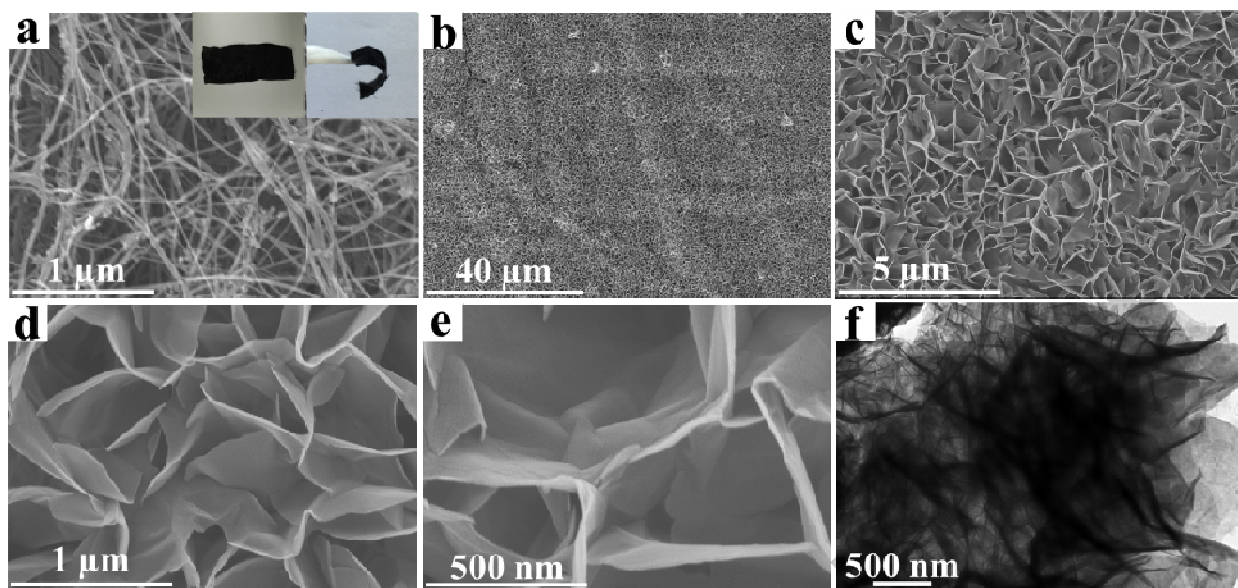


Fig. 2 Typical SEM images of (a) CNP and (b-e) CNP-LDH, and (f) TEM image of NiAl-LDH scraped from CNP-LDH by mild sonication.

ACCEPTED MANUSCRIPT

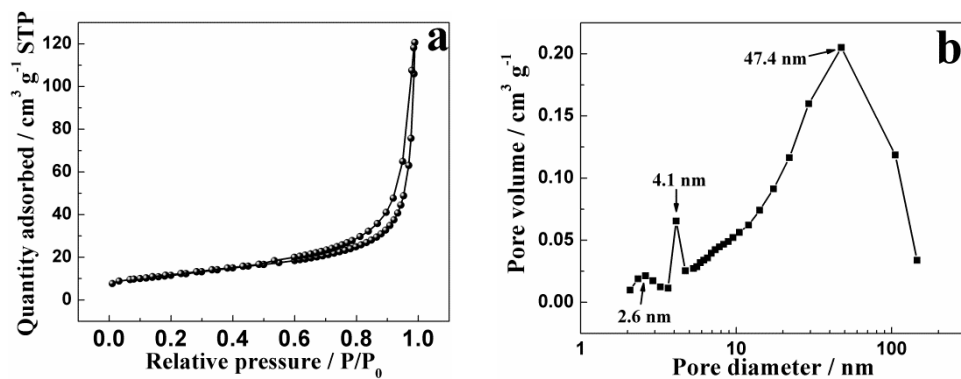


Fig. 3 (a) The nitrogen adsorption-desorption isotherm loop and (b) the pore size distribution data of NiAl-LDH scraped from CNP-LDH by mild sonication.

ACCEPTED MANUSCRIPT

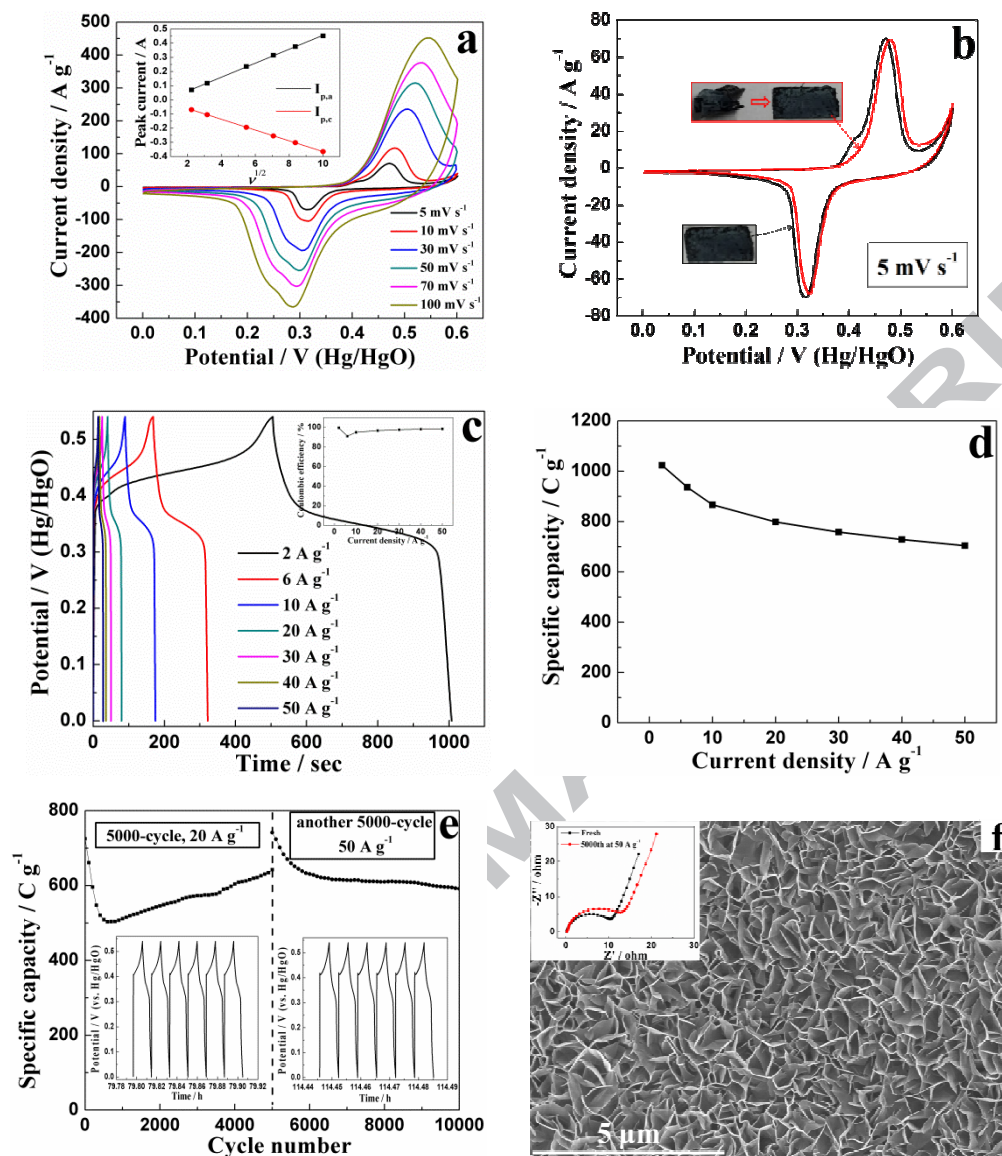


Fig. 4 (a) CV curves of CNP-LDH electrode at various scan rates (inset: relationship of peak current with scan rate). (b) Comparison of CV curves of CNP-LDH electrode and after crumpling into a ball (scan rate: 5 mV s^{-1}). (c) GCD curves of CNP-LDH electrode at different current densities (inset: Coulombic efficiency of CNP-LDH electrode at different current densities). (d) Correlation between the specific capacity values and current density of CNP-LDH electrode. (e) Cycling performance of the electrode at current densities of 20 A g^{-1} and 50 A g^{-1} for 5000 cycles, respectively. (f) SEM image of CNP-LDH electrode after the cycling stability test (inset: electrochemical impedance spectra of CNP-LDH before and after cycling test).

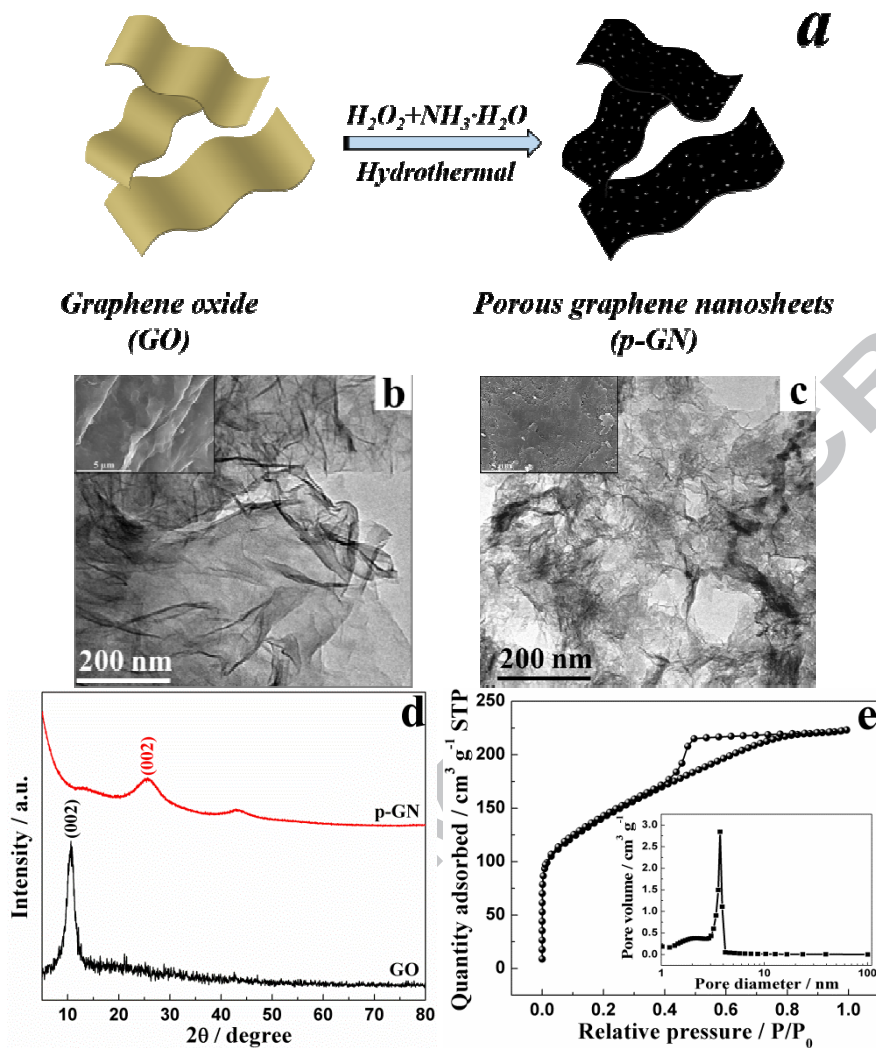


Fig. 5 (a) Schematic illustration of the synthesis of p-GN material. Typical TEM and SEM images of (b) GO and (c) p-GN. (d) XRD pattern of GO and p-GN. (e) The nitrogen sorption isotherm loop and the pore size distribution data of p-GN.

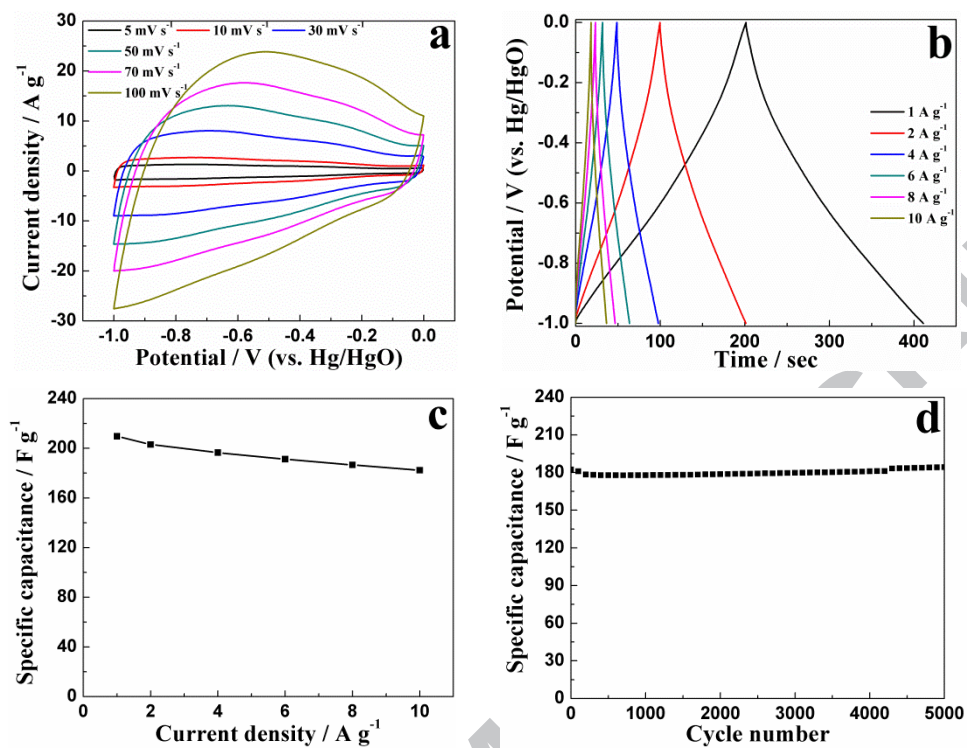
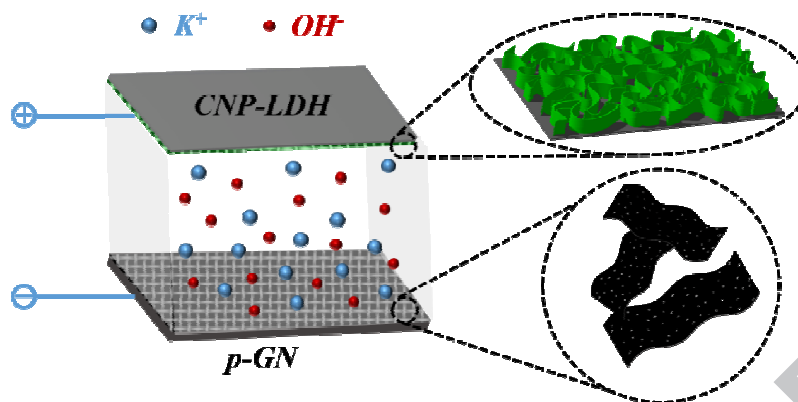


Fig. 6 (a) CV curves of p-GN electrode at various scan rates. (b) Charge-discharge curves of p-GN electrode at different current densities. (c) Specific capacitance of p-GN electrode at different current densities. (d) Cycling stability of p-GN electrodes at 10 A g⁻¹ for 5000 cycles.



Scheme 1 The HSC made of CNP-LDH (positive electrode) // p-GN (negative electrode).

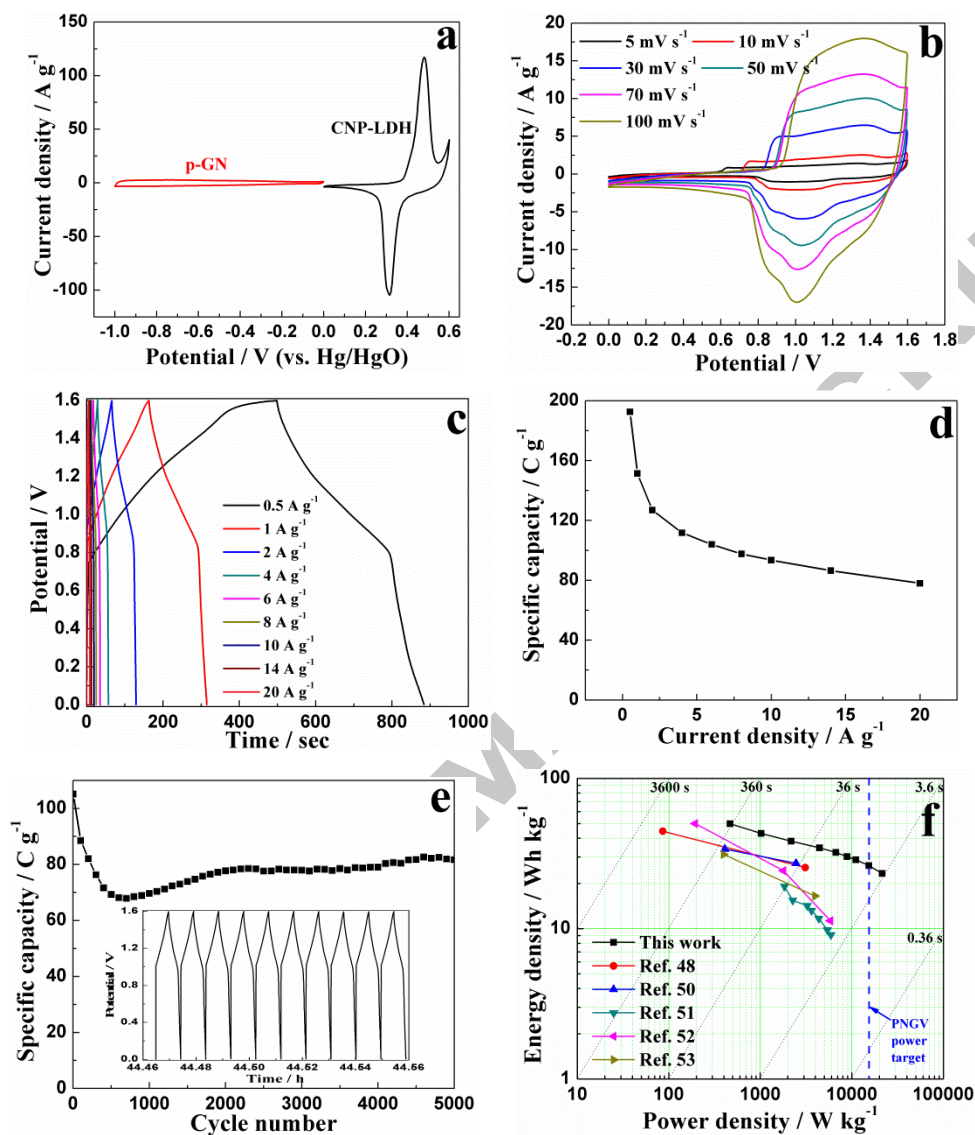
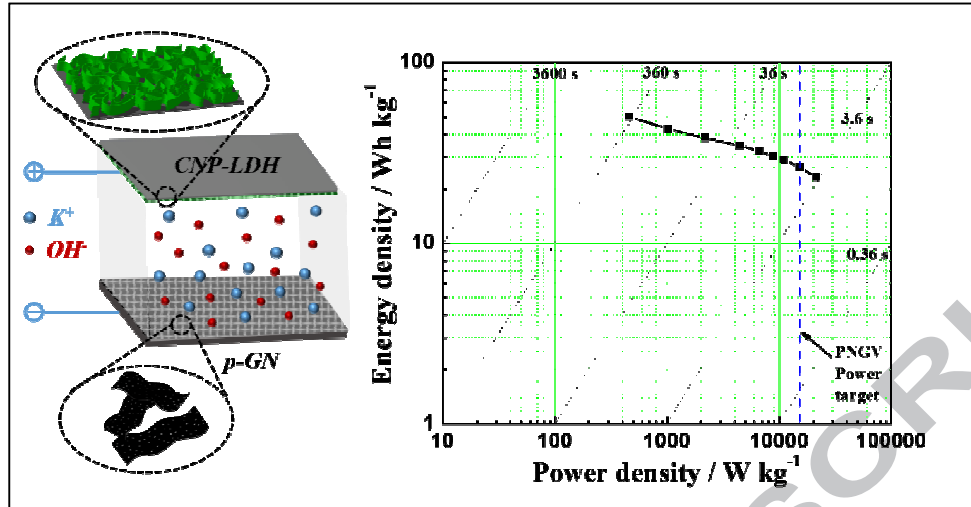


Fig. 7 (a) CV curves of CNP-LDH and p-GN in a three-electrode system at a scan rate of 10 mV s⁻¹. (b) CV curves of CNP-LDH/p-GN HSC device at different scan rates. (c) GCD curves and (d) specific capacity of HSC device at different current densities. (e) Cycling performance of HSC device at 5 A g⁻¹ for 5000 cycles. (f) Ragone plot of energy and power density of HSC device at various charge-discharge rates.

- > Layered double hydroxide is grown on carbon nanotube paper as positive electrode.
- > Porous graphene nanosheets with high performance are used as negative electrode.
- > The hybrid supercapacitor shows high energy density and superior power density.

ACCEPTED MANUSCRIPT



ACCEPTED MANUSCRIPT